SAND2015-1663C

# Trapping Characteristics and Parametric Shifts in Lateral GaN HEMTs with $SiO_2$/AlGaN Gate Stacks

M. P. King, J. R. Dickerson, S. DasGupta, M. J. Marinella, and R. J. Kaplar
Sandia National Laboratories
Albuquerque, NM, 87111 USA
mpking@sandia.gov

D. Piedra, M. Sun, and T. Palacios
Massachusetts Institute of Technology
Cambridge, MA 02139, USA

*Abstract*—**Recovery transients following blocking-state voltage stress are analyzed for two types of AlGaN/GaN HEMTs, one set of devices with thick AlGaN barrier layers and another with recessed-gate geometry and ALD $SiO_2$ gate dielectric. Results show temperature-invariant emission processes are present in both devices. Recessed-gate devices with $SiO_2$ dielectrics are observed to exhibit simultaneous trapping and emission processes during post-stress recovery.**

***Keywords- gallium nitride, HEMT, current collapse, defects, trapped charge, power electronics, reliability***

## I. INTRODUCTION

High voltage AlGaN/GaN HEMTs has seen widespread application in power and RF electronics. Low on-state resistance due to high channel mobility at the AlGaN/GaN heterointerface coupled with high critical field for breakdown in the III-N system ($E_C \approx 3$ MV/cm for GaN) has led to significant progress in developing the AlGaN/GaN HEMT as a high-voltage device for next-generation switching power electronics. However, many issues specific to AlGaN/GaN HEMT reliability remain unresolved and are poorly understood. In particular, properties and locations of defects in the AlGaN/GaN material system and how these defects impact performance at the device- and circuit-level are important factors in developing power devices with both improved performance and reliability [1]–[3].

In this work, we investigate and compare the trapping properties of AlGaN/GaN HEMTs with recessed gates and $SiO_2$ gate dielectrics to those with thicker AlGaN barrier layers and no $SiO_2$ present. Drain current transients were analyzed following blocking-state stress ($V_{gs} < V_{th}$, $V_{ds} = 100$ V) and these transients, believed to be due to electron emission, exhibit strong stress-time-dependent behavior. Extracted time constant spectra demonstrate that a temperature-independent component becomes progressively slower as the stress time is increased. Recessed-gate devices with $SiO_2$ gate dielectrics exhibit both negative and positive transient components representative of simultaneous trapping and emission processes, where carrier trapping dominates at short recovery times and emission is prominent at longer recovery times.

Sandia National Laboratories is a multi-program laboratory managed and operated by Sandia Corporation, a wholly owned subsidiary of Lockheed Martin Corporation, for the U.S. Department of Energy's National Nuclear Security Administration under contract DE-AC0494AL85000. The Sandia work was performed under funding from SNL's Laboratory Directed Research and Development Program. The MIT work was partially funded by the DARPA DAHI program, monitored by Dr. Daniel Green, and the ONR DEFINE MURI, monitored by Dr. Paul Maki.

## II. EASE OF USE

Two device variants are investigated in this work. All of the tested devices were fabricated at Massachusetts Institute of Technology on silicon (111) substrates. Device type A had gate-to-drain spacing $L_{gd}$ ranging from 1.5 to 40 µm, gate-to-source spacing $L_{gs}$ = 1.5 µm, and gate length $L_g$ = 2 µm. These devices used $Al_{0.15}Ga_{0.85}N$ for the 50 nm thick barrier and had a threshold voltage ($V_{th}$) of −4.1 V. Type A HEMTs used 4 µm epilayers with a carbon-doped 2.4 µm buffer and 1.4 µm of *i*-GaN, and the channel GaN was 200 nm thick. The surface passivation was an $Al_2O_3/SiO_2/Al_2O_3$ stack grown by atomic layer deposition, and was deposited after the gate. A few monolayers (< 2 nm) of gallium oxide, resulting from oxygen plasma treatment before gate pattering, act as the gate dielectric. No field plates were used in the structure. Device type B, shown in Fig. 1, was fabricated with an 18 nm thick $Al_{0.26}Ga_{0.74}N$

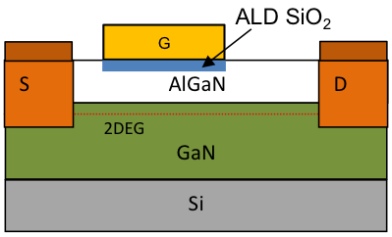


Fig. 1. Device type B schematic cross section. The AlGaN barrier is etched

barrier, 1.2 μm of GaN, and a 2.8 μm buffer. These devices had $L_{gs}$ = 2 μm, $L_{gd}$ varied from 10 μm to 22 μm, and $L_g$ was 2 μm. The type B devices have an $SiO_2$ (deposited by ALD) gate dielectric with a thickness of 18.6 nm. The surface is passivated with a 190 nm thick SiN layer deposited by PECVD, and a source-connected field plate is present.

## III. Experimental and Analytical Methods

In this work, a modified current transient analysis method [4] with regularization techniques [5], [6] was used to characterize the recovery transients. We note that current transient methods are conceptually similar to the approach of Grasser in [7] with comparable techniques applied by Lagger in [8] to HEMT structures. In the current transient method of Joh and del Alamo [4], an experimental recovery transient, $\Delta I_d(t) = I_d(t) - I_d(0)$, is analyzed by fitting to a sum of exponentials of the form

$$\Delta I_d = \sum \alpha_i \left(1 - e^{-t/\tau_i}\right) \tag{1}$$

where $\alpha_i$ is the coefficient of a process associated with time constant $\tau_i$. As constructed in Eq. (1), positive values for $\alpha_i$ correspond to emission processes while negative values correspond to capture processes.

Simultaneously determining a set of $\alpha_i$ and $\tau_i$ is a notoriously ill-posed mathematical problem, specifically, a Type II Fredholm integral problem [5]. Due to the non-orthogonal nature of the multi-exponential model constructed to represent the device recovery characteristics, Fourier techniques fail to reconstruct the spectral response without large comprises made in terms of resolution [9]. In [1], [2], and [4], a method for reconstructing recovery transients was presented that used non-linear optimization techniques to fit recovery transients to experiment. This technique results in an emission spectrum corresponding to the detrapping of carriers during device relaxation in the *on*-state. Each of these studies used a regularization term, specifically a second term in the minimization problem containing the time derivative of the fitted transient, to penalize additional terms and recover Inclusion of the time derivative in the minimization problem of [1], [2], and [4] has two consequences. First, it results in a non-linear optimization problem that becomes computationally expensive with increasingly large data sets. Second, it imposes artificial smoothness on the solution, causing peaks in the resulting emission spectrum to be broad in nature and results in a lack of resolution, obscuring any neighboring peaks below a given threshold magnitude. Instead, this work notes that other fields have devoted significant effort to model multi-exponential systems and have developed codes that approach the problem in an efficient manner. CONTIN, a FORTRAN code written by Provencher [5], has seen widespread use in the fields of nuclear physics, chemistry, and medicine (nuclear magnetic resonance and magnetic resonance imaging) [10], semiconductor physics in the form of Laplace deep level transient spectroscopy (L-DLTS) [11], biology in the analysis of protein structure [12], [13], and astronomy in the analysis of scattered light [10], [14]. This work has developed a new code

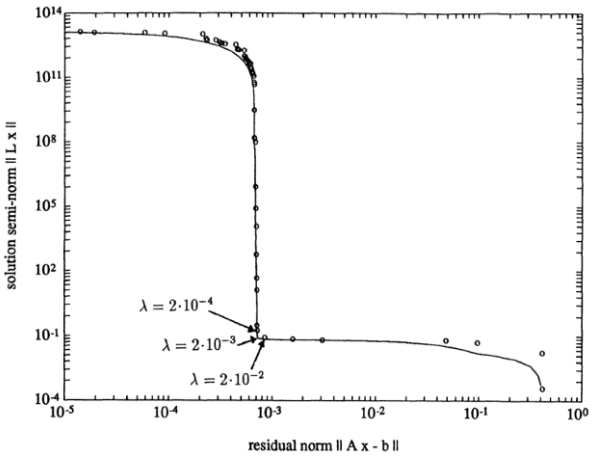


Fig. 2. The Tikhonov L-curve shows the optimal choice of λ resides at the balance between the magnitude of the norm of the least-squares and regularization term. After [15].

based on CONTIN that performs an adaptive determination of multi-exponential systems in Python. The approach taken by CONTIN and in our modified current transient method used here imposes the principle of parsimony and can be described by

$$y_{fit} = \min\left(|y - A\alpha|^2 + \lambda \left|\frac{d^2}{dt^2} A\alpha\right|^2\right) \tag{2}$$

where $y$ is the recovery transient and $A\alpha$ is the estimation of $y$.

Of note in Eq. (2) is the form of the regularization term. Inclusion of the second time derivative of the approximation imposes a condition of curvature, forcing the solution to be twice continuously differentiable. This results in a Gaussian-like peak corresponding to time constants of significant spectral components. Gaussian peaks have a distinct advantage over the smoothness imposed in [1], [2], and [4] in that they have a sharp δ-like presentation, which in turn will be shown to lead to increased resolution [5]. The second important term in the regularization term is the $\lambda$ weighting factor, which weights the relative importance of the regularization term in the solution. This dynamic factor prevents either the least-squares component or the second derivative term from dominating the solution space, resulting in a spectrum that favors neither the least squares nor the second derivative, but properly considers each when reconstructing a recovery transient solution. This behavior can be seen in Fig. 2, known as an L-curve in regularization techniques [15], where the least squares and regularization terms are shown to have an optimal point where $\lambda$ weights the regularization term appropriately and results in the best approximation of the solution even in the presence of significant noise. We note that any solution of a single-shot measurement that involves the use of derivatives in its approximation is inherently noisy, making the use of a weighting term beneficial in this analysis method. Consequently, in our construction of this analysis technique, $\lambda$ is a dynamic term that iteratively weights the regularization term of a minimization solving routine to achieve the optimal solution of a recovery transient.

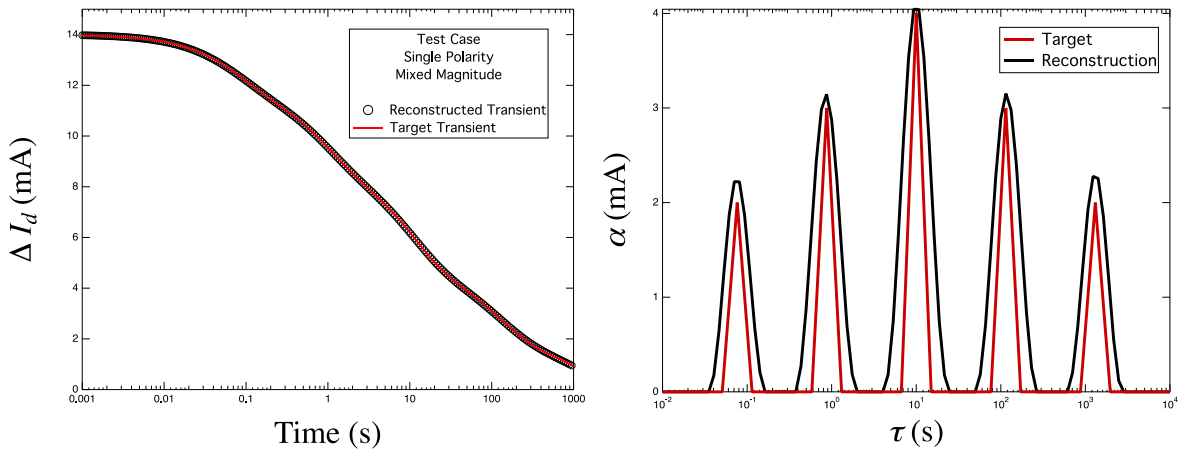


Fig. 3. Test case example of the modified current-transient method for evaluating device recovery transients featuring only emission processes. (a) Time-domain signal of an artificial current transient with all positive components and (b) corresponding time-constant spectrum extracted from our method. Results show the time-constant spectrum is reconstructed with great accuracy, in both temporal resolution and magnitude of spectral components.

Lastly, prior to the application of our modified current transient technique, a series of numerical methods are applied to determine the polarity and magnitude of the bounds for each $\alpha_i$ and $\tau_i$ pair. These constraints are passed to an appropriate solver that considers the sign and magnitude of a solution when minimizing the non-linear optimization problem of Eq. (2). The quasi-newton approach of the limited-memory BFGS method [16], [17] is particularly advantageous due to its fast convergence and handling of the Hessian matrix, allowing it to operate on large data sets while maintaining the appropriate boundary conditions determined in previous numerical evaluation that impose so-called "prior knowledge" on the solution.

To validate this approach, we construct several sets of artificial recovery transients as test cases for the method. These case studies are intended to show the robust nature and idealized behavior of the solution to a known problem and determine the limitations of this approach. The results of this effort can be seen in Fig. 3 and Fig. 4. Fig. 3 shows the time- (a) and spectral-domain (b) for an artificial recovery transient where only emission processes contribute to the device response (all $\alpha_i$ are positive). Fig. 3 (a) shows the transient response can be accurately represented using the sum of exponentials using the method described in Eq. (2) over a large time domain. The corresponding time constant spectrum can be seen in Fig. 3 (b), which shows the adaptive regularization method used here results in a solution that very accurately reconstructs the original, artificial time constant spectrum, resulting in precise magnitude and temporal agreement between the target (artificial) sample and the numerical approximation.

The second test case is shown in Fig. 4 and represents a transient with mixed polarity of the spectral components, representative of concurrent capture and emission processes. Fig. 4 (a) again shows the time-domain representation of the artificial recovery transient and the reconstructed transient using the methods described in this section. Excellent agreement is obtained in the time-domain signal for this difficult test case, which to our knowledge has not previously been demonstrated. Similarly, the time constant spectrum reconstruction of this artificial transient agrees very well with the intended solution as shown in Fig. 4 (b). The Gaussian-like

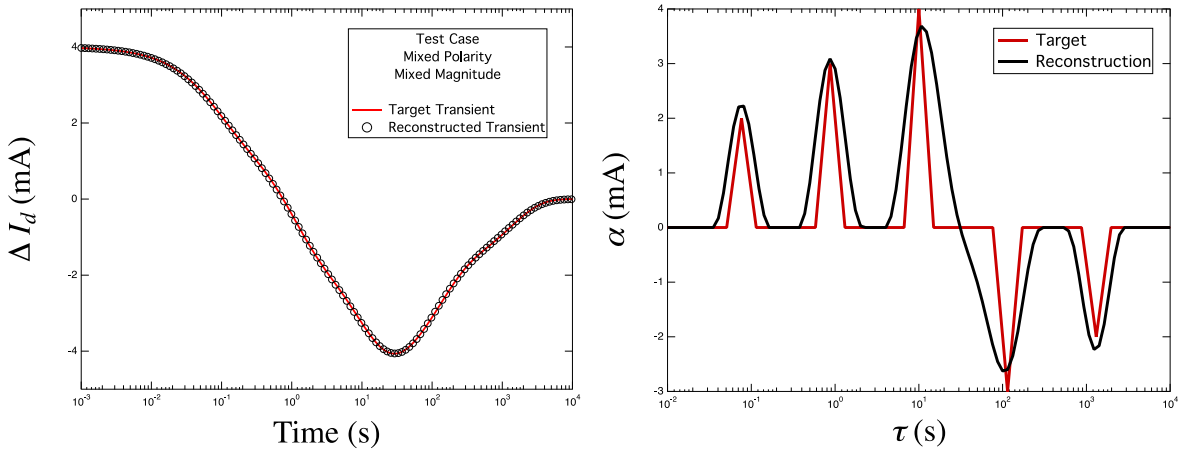


Fig. 4. Test case example of the modified current-transient method for evaluating device recovery transients featuring both emission and capture processes. (a) Time-domain signal of an artificial current transient with positive and negative components and (b) corresponding time-constant spectrum extracted from our method. Results show the time-constant spectrum is reconstructed with great accuracy including this difficult test case, showing excellent temporal resolution and magnitude of spectral components.

peaks appear at the appropriate time constants and are of approximately the correct magnitude, with the exception of the region where spectral components switch from positive to negative. This transition region is difficult to define using numerical derivative methods and results in a loosely bounded region for solutions. As a result, our method approximates peaks at the correct time constants and reduces the corresponding magnitudes to account for solutions in the loosely bound region. This represents a worst-case situation for any regularization method. Another worst case would involve multiple peaks at time constants within a factor of 2; here the method tends to average the solution into a single peak. The practicality of these worst-case examples is debatable since one would not expect to find a large number of traps with similar emission time constants. We note the lack of oscillatory behavior in the solutions of Fig. 3 and Fig. 4 as an improvement over previous methods, where solutions sometimes indicate the presence of detrapping processes at time constants not corresponding to any physically reasonable time- or temperature-varying trapping processes.

To summarize, the treatment in Eq. (2) allows imposing curvature and prior knowledge on solutions while penalizing over-fitting, resulting in a well-behaved time-domain and spectral representation. The method uses mathematical techniques that have been well-studied and established in a wide variety of fields. Next, we apply this method to the analysis of recovery transients in stressed AlGaN/GaN HEMTs.

## IV. Analysis of Off-State Stress Recovery

The devices described in Section II were measured in complete darkness under blocking *off*-state stress conditions ($V_{gs}$ = -5 V, $V_{ds}$ = 100 V). Stress was applied for variations of 1, 10, and 100 s at temperatures of 300, 315, and 330 K. Following stress, recovery transients were recorded in the *on*-state ($V_{ds}$ = 0.1 V, $V_{gs}$ = 1 V). Prior to stress, the drain current $I_D$ and threshold voltage $V_{th}$ was completely recovered to the initial fresh-device value by shining the probe station microscope halogen lamp on the sample and allowing the device to relax for 300 seconds. Consequently, the effects to be discussed are related to variations in occupancy of traps that existed prior to any electrical stress. The complete recovery of both $I_d$ and $V_{th}$ indicate there was no permanent device degradation due to the electrical stress conditions.

### A. Results from AlGaN/GaN HEMTs

First, we analyze recovery transients obtained following *off*-state stress for device type A, a more traditional AlGaN/GaN HEMT. Stress-recovery results can be seen in Fig. 5 and Fig. 6. Fig. 5 (a) shows the stress time dependence of recovery transients at 300 K. Increasing stress time $t_{str}$ is results are consistent with electron trapping, either in the AlGaN barrier [2], [4] or in the GaN bulk [18], which causes a

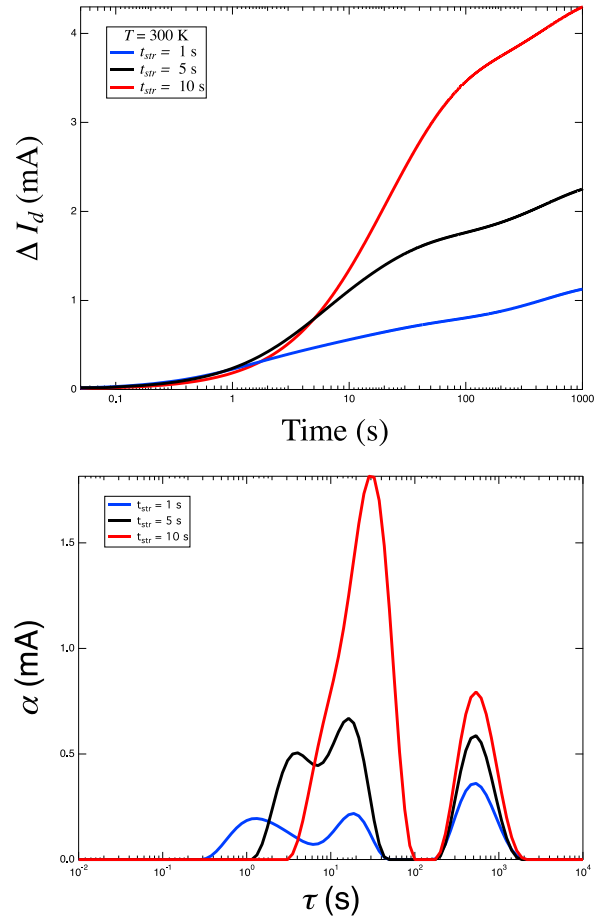


Fig. 5. Device type A recovery transient analysis results reveal a temperature-invariant process that becomes slower and increases in magnitude with increasing stress time (T = 300 K).

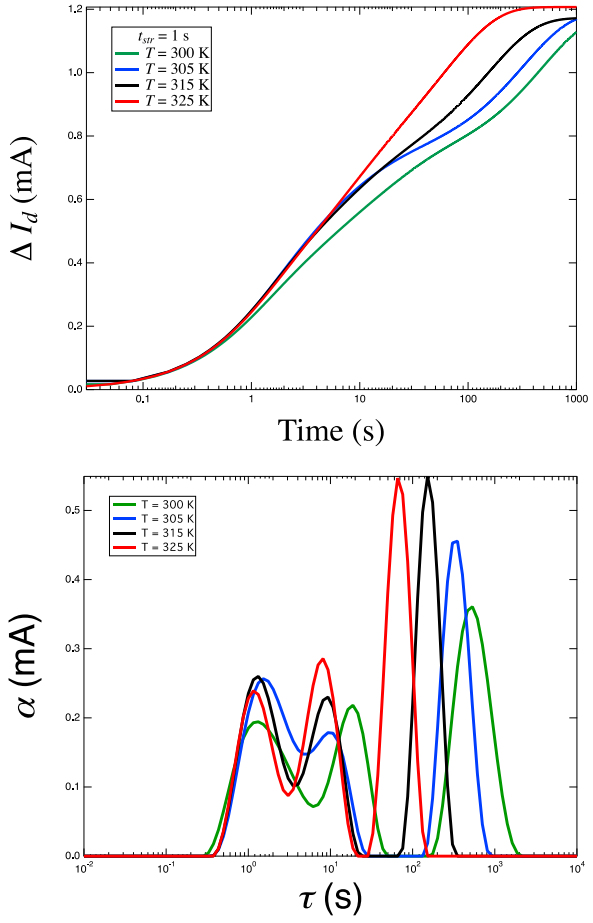


Fig. 6. Device type A recovery transient results reveal a slow temperature dependent component ($t_{str}$ = 1 s) with $E_a \approx 0.57$ eV.

change in threshold voltage as reported in previous work.

Next, we use our modified current transient method to analyze the stress-recovery transient behavior of these devices; the resulting time constant spectra from this analysis are shown in Fig. 5 (b). Several features are present in each of the spectra shown, one associated with large $\tau$, which is more δ-like, and a broad distribution at smaller $\tau$. We observe that the emission process associated with small $\tau$ shifts to larger $\tau$ and increases in magnitude with increasing $t_{str}$. For $t_{str}$ greater than 1 s, the processes associated with this broad peak increase in magnitude and become the dominant component of the recovery transient spectrum response. The physical mechanisms associated with this temperature-invariant, stress-time-related emission process are still under investigation. At short times (< 1 s), the recovery transient behavior of this device stressed for 10 s shows less recovery than devices stressed for 1 and 5 s. This is reflected in the time constant spectrum of Fig. 5 (b) which shows that the stress-time dependent emission process becomes progressively slower and stronger.

These measurements were repeated on device type A with temperature varying from $T$ = 300 to 325 K and $t_{str}$ = 1 s and can be seen in Fig. 6. Recovery transients are observed to exhibit dependence on temperature in Fig. 6 (a), where for increasing temperature the devices recover progressively faster to their nominal $I_d$ value. The transient recovered at $T$ = 325 K is shown to completely recover within 300 s, while at lower temperature devices recover most (but not all) of their pre-stress $I_d$.

The analysis of these transients yields the time constant spectrum shown in Fig. 6 (b). The same features are present in these spectra as in Fig. 5 (b), a broad component at smaller $\tau$ and a larger δ-like component at larger $\tau$. The stress-time dependent peak from Fig. 5 (b) is observed to be relatively insensitive to temperature over the range of temperatures shown in these spectra and is suspected to be related to the presence of a deep level state in the AlGaN barrier. The feature present at larger $\tau$ exhibits a temperature dependence and is seen to shift to smaller time constants with increasing temperature. Analysis of these peaks yields activation energy $E_a$ = 0.57 eV below the conduction band edge, consistent with a commonly reported trap energy in GaN and AlGaN/GaN material systems. These results are consistent with previous reports of slow detrapping processes in AlGaN/GaN HEMTs [2].

### *B. Results from MOS-HEMTs*

Next, we investigate the stress-recovery behavior of device type B, a recent generation MOS-HEMT fabricated at MIT, with *off*-state stress conditions $V_{gs}$ = -5 V and $V_{ds}$ = 100 V and *on*-state recovery recorded at $V_{gs}$ = 1 V and $V_{ds}$ = 0.1 V for stress times of $t_{str}$ = 1 s and 100 s. Prior to each stress-recovery measurement, the device was exposed to the probe station halogen lamp for a period of 300 s with 0 V applied to all device terminals, allowing the device to completely recover in both $I_d$ and $V_{th}$. The results of these measurements are shown in Fig. 7 and are representative of many of the devices evaluated in this work.

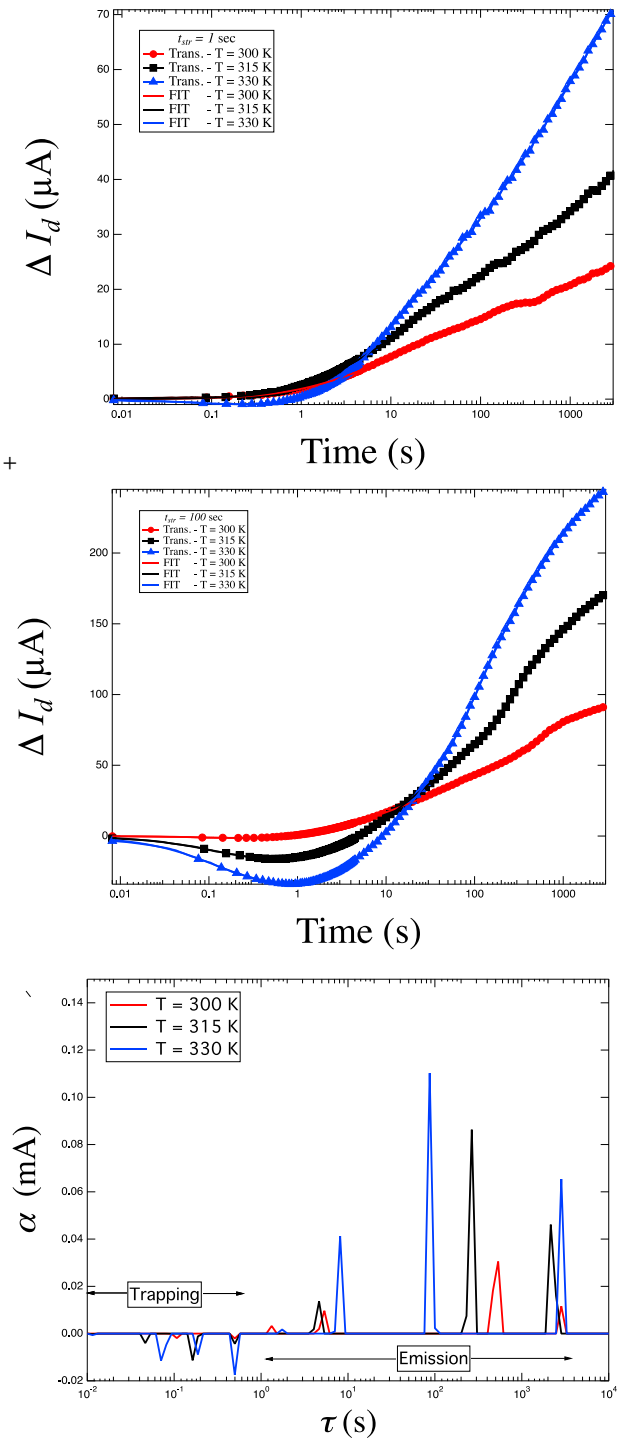


Fig. 7. (a) Recovery transients for $t_{str}$ = 1 s show the impact of temperature and stress on device operating conditions; increasing temperature results in higher degradation of $I_D$ for equivalent stress times. Similarly, (b) $t_{str}$ = 100 s yields higher $I_D$ loss; however, a continued degradation of $I_D$ is initially observed prior to recovery of the device. Analysis (c) of these transients shows simultaneous trapping and emission processes.

Fig. 7 (a) shows a set of recovery transients following 1 s *off*-state stress for temperature conditions of 300, 315, and 330

K. The recovery transient behavior is consistent with previous results from [2] and [4] and are easily attributable to emission of carriers from trapping centers in and near the MOS-AlGaN barrier layer and interfaces.

First, we observe that for the MOS-HEMT devices studied here (device type B), *off*-state stress for $t_{str}$ = 1 s results in significantly less change in both $\Delta V_{th}$ and $\Delta I_d$, as seen in Fig. 7 (a), as compared to the more traditional Schottky-gated device type A reported in the previous section. For longer stress time, $t_{str}$ = 100 s, the same observation is made, as seen in Fig. 7 (b). Even for longer stress times the $\Delta I_d$ for MOS-HEMT devices is consistently observed to be less than 20% of what is observed in Schottky-gated devices. The reduction in $\Delta V_{th}$ and $\Delta I_d$ following *off*-state stress for the MOS-HEMT devices indicates that the presence of the $SiO_2$ in the device barrier layer plays a significant role in suppressing the trapping of carriers during stress and subsequent device relaxation during recovery.

Recovery transients shown in Fig. 7 (a) and (b) each show that for increasing temperature the magnitude of $\Delta I_d$ recovery also increases, suggesting another temperature dependent component in the time constant spectra associated with these transients. A distinguishing feature of recovery transients from the MOS-HEMT devices is that even at T = 330 K no saturation is observed of these devices. This suggests an increased barrier to emission preventing the complete recovery of $\Delta I_d$ and $\Delta V_{th}$ back to their nominal, pre-stress values on the time scales during which device recovery was monitored.

At $T$ = 330 K, Fig. 7 (a) shows that recovery transients following 1 s *off*-state stress exhibit a magnitude of $I_d$ recovery below that of equivalent stress-time measurements at $T$ = 300 and 315 K until approximately 10 s have elapsed. This behavior is observed again for longer *off*-state stress time of 100 s, as shown in Fig. 7 (b). Here, the recovery transient response shows an initial decrease in $I_d$ following the removal of stress and begins to recover back towards its pre-stress condition after approximately 10 s. Current transient analysis is performed on the MOS-HEMT devices with the results shown in Fig. 7 (c). The time constant spectra shown in Fig. 7 (c) for the MOS-HEMT devices show similar features to those observed in the Schottky-gated HEMT devices reported in Section IV B. Our full analysis reveals the same stress-time dependent emission process between $\tau$ = 1 s and 20 s, and a larger temperature-dependent component at $\tau$ > 100 s. Similar analysis of the temperature dependent peak reveals a trap with activation energy $E_a$ = 0.56 eV below the conduction band edge.

The initial decrease in $\Delta I_d$ in Fig. 7 (a) and (b) is observed as an exponential process in our analysis represented negative magnitude peaks in the time constant spectra of Fig. 7 (c). These results strongly suggest the presence of simultaneous trapping and emission processes occurring within the same recovery transient, leading to the behavior observed in Fig. 7 (a) and (b). The nature of these concurrent processes will be discussed in the following section.

### *C. Discussion*

Understanding of the band diagram structure has been useful in previous studies of the trapping behavior of Schottky-gated HEMTs. Here, we consider the band structure of the MOS-HEMT in an attempt to understand the nature of the trapping behavior observed in Fig. 7.

The band diagram of a MOS-HEMT in the *off*- and *on*-state conditions is shown in Fig. 8 (a) and (b) respectively. In the *off*-state, the bands are bent up, forcing electrons to migrate from the heterointerface towards the bulk of the material. This leads to filling of traps in the GaN buffer region of the device. Simultaneously, electrons are injected from the gate electrode into the $SiO_2$ barrier layer. Due to the thickness of the oxide (19 nm), it is unlikely that carriers will tunnel completely through it into the AlGaN region. Typically, $SiO_2$ is regarded as having a tendency to trap net positive charge due to the predominance of hole traps and associated low mobility. This is characteristic of thermally grown oxides, and it is unclear

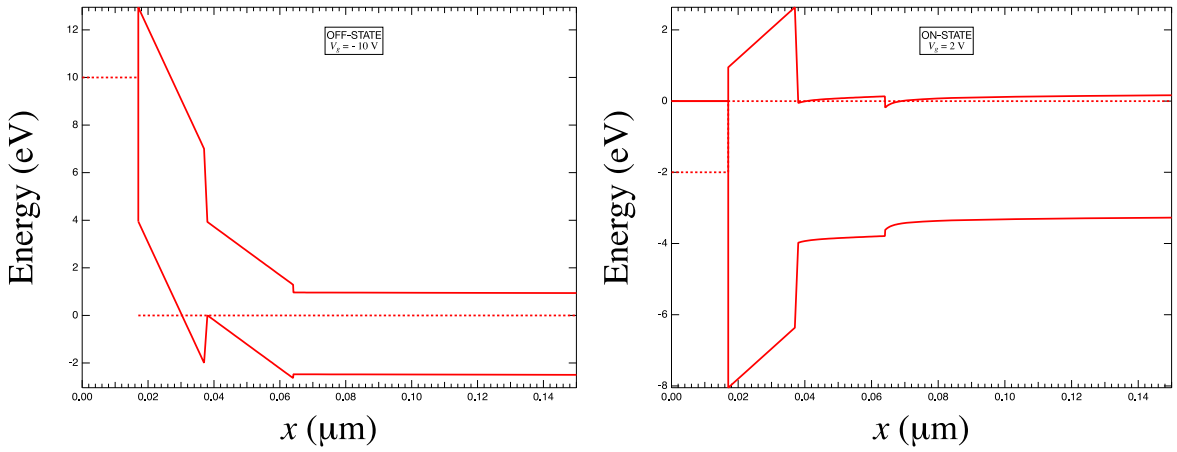


Fig. 8. Energy band diagrams for the MOS-HEMT (device type B) structures. These devices have 19 nm ALD $SiO_2$ and 18 nm AlGaN as a gate stack. In the *off*-state (a), the channel is shown to be depleted, and carriers are injected from the gate into the $SiO_2$, leading to a positive $\Delta V_{th}$ and reduction in $I_d$. Switching to the *on*-state (b) leads to quick filling of empty traps in the AlGaN barrier and at the AlGaN/GaN interface, resulting in a current collapse-like response of the device. This is overcome eventually by the emission of trapped electrons from the $SiO_2$ layer and leads to recovery of $V_{th}$ and $I_d$ towards their nominal values.

whether this behavior translates to the ALD $SiO_2$ here. It is quite possible that injected electrons can be trapped or reduce the net positive charge in the ALD $SiO_2$ layer, leading to a positive $\Delta V_{th}$ and a corresponding reduction in $I_d$ during *off*-state stress conditions.

The change of operating condition from *off* to *on* results in a change in the band bending and accumulation of electrons to the heterointerface. In this case, we have an AlGaN barrier layer that was not readily exposed to a source of electrons during stress and consequently, most of the traps in this layer are empty prior to switching to the *on*-state condition. As a consequence of the empty trap states in the AlGaN, when carriers aggregate at the AlGaN/GaN interface they quickly occupy interface states, again resulting in a net positive $\Delta V_{th}$ and reduction in $I_d$. This effect is temporary, since the field in the oxide layer begins to slowly detrap electrons that were previously injected during *off*-state stress, and leads to the gradual recovery of both $V_{th}$ and $I_d$. That this effect takes approximately 10 seconds to become evident in the device response can be explained by the competition between trapping and detrapping processes occurring simultaneously in different layers of the $SiO_2$-AlGaN barrier region.

## V. Conclusions

In this work, we have presented an improved method for analyzing the recovery of slow-detrapping transients following stress. This method was used to investigate and compare the stress-recovery charge trapping and detrapping properties of Schottky-gated HEMTs with MOS-HEMT devices. Drain current transients were analyzed following *off*-state stress ($V_{gs} < V_{th}$, $V_{ds}$ = 100 V) and these transients, believed to be due to electron emission, exhibit strong stress-time-dependent behavior. Extracted time constant spectra demonstrate that a temperature-independent component becomes progressively slower as the stress time is increased. MOS-HEMT devices with $SiO_2$ gate dielectrics exhibit both negative and positive transient components representative of simultaneous trapping and emission processes, where carrier trapping dominates at short recovery times and emission is prominent at longer recovery times.

## References


[1] S. DasGupta, L. B. Biedermann, M. Sun, R. Kaplar, M. Marinella, K. R. Zavadil, S. Atcitty, and T. Palacios, "Role of barrier structure in current collapse of AlGaN/GaN high electron mobility transistors," *Appl. Phys. Lett.*, vol. 101, no. 24, p. 243506, Dec. 2012.

[2] S. DasGupta, M. Sun, A. Armstrong, R. J. Kaplar, M. J. Marinella, J. B. Stanley, S. Atcitty, and T. Palacios, "Slow Detrapping Transients due to Gate and Drain Bias Stress in High Breakdown Voltage AlGaN/GaN HEMTs," *IEEE Trans. Electron Devices*, vol. 59, no. 8, pp. 2115–2122, Aug. 2012.

[3] A. R. Arehart, A. Sasikumar, S. Rajan, G. D. Via, B. Poling, B. Winningham, E. R. Heller, D. Brown, Y. Pei, F. Recht, U. K. Mishra, and S. A. Ringel, "Direct observation of 0.57 eV trap-related RF output power reduction in AlGaN/GaN high electron mobility transistors," *Solid-State Electron.*, vol. 80, pp. 19–22, Feb. 2013.

[4] J. Joh and J. A. del Alamo, "A Current-Transient Methodology for Trap Analysis for GaN High Electron Mobility Transistors," *IEEE Trans. Electron Devices*, vol. 58, no. 1, pp. 132–140, Jan. 2011.

[5] S. W. Provencher, "A constrained regularization method for inverting data represented by linear algebraic or integral equations," *Comput. Phys. Commun.*, vol. 27, no. 3, pp. 213–227, Sep. 1982.

[6] A. N. Tikhonov, *Numerical Methods for the Solution of Ill-Posed Problems*. Springer, 1995.

[7] T. Grasser, H. Reisinger, P.-J. Wagner, and B. Kaczer, "Time-dependent defect spectroscopy for characterization of border traps in metal-oxide-semiconductor transistors," *Phys. Rev. B*, vol. 82, no. 24, p. 245318, Dec. 2010.

[8] P. Lagger, M. Reiner, D. Pogany, and C. Ostermaier, "Comprehensive Study of the Complex Dynamics of Forward Bias-Induced Threshold Voltage Drifts in GaN Based MIS-HEMTs by Stress/Recovery Experiments," *IEEE Trans. Electron Devices*, vol. 61, no. 4, pp. 1022–1030, Apr. 2014.

[9] S. W. Provencher, "A Fourier method for the analysis of exponential decay curves.," *Biophys. J.*, vol. 16, no. 1, pp. 27–41, Jan. 1976.

[10] A. A. Istratov and O. F. Vyvenko, "Exponential analysis in physical phenomena," *Rev. Sci. Instrum.*, vol. 70, no. 2, pp. 1233–1257, Feb. 1999.

[11] L. Dobaczewski, A. R. Peaker, and K. B. Nielsen, "Laplace-transform deep-level spectroscopy: The technique and its applications to the study of point defects in semiconductors," *J. Appl. Phys.*, vol. 96, no. 9, pp. 4689–4728, Nov. 2004.

[12] S. W. Provencher and J. Gloeckner, "Estimation of globular protein secondary structure from circular dichroism," *Biochemistry (Mosc.)*, vol. 20, no. 1, pp. 33–37, 1981.

[13] P. J. Steinbach, R. Ionescu, and C. R. Matthews, "Analysis of Kinetics Using a Hybrid Maximum-Entropy/Nonlinear-Least-Squares Method: Application to Protein Folding," *Biophys. J.*, vol. 82, no. 4, pp. 2244–2255, Apr. 2002.

[14] S. W. Provencher and P. Štěpánek, "Global Analysis of Dynamic Light Scattering Autocorrelation Functions," *Part. Part. Syst. Charact.*, vol. 13, no. 5, pp. 291–294, 1996.

[15] P. Hansen, "Analysis of Discrete Ill-Posed Problems by Means of the L-Curve," *SIAM Rev.*, vol. 34, no. 4, pp. 561–580, Dec. 1992.

[16] R. Byrd, P. Lu, J. Nocedal, and C. Zhu, "A Limited Memory Algorithm for Bound Constrained Optimization," *SIAM J. Sci. Comput.*, vol. 16, no. 5, pp. 1190–1208, Sep. 1995.

[17] C. Zhu, R. H. Byrd, P. Lu, and J. Nocedal, "Algorithm 778: L-BFGS-B: Fortran Subroutines for Large-scale Bound-constrained Optimization," *ACM Trans Math Softw*, vol. 23, no. 4, pp. 550–560, Dec. 1997.

[18] A. Sasikumar, D. W. Cardwell, A. Arehart, J. Lu, S. W. Kaun, S. Keller, U. K. Mishra, J. S. Speck, J. P. Pelz, and S. . Ringel, "Toward a physical understanding of the reliability-limiting EC-0.57 eV trap in GaN HEMTs," in *Reliability Physics Symposium, 2014 IEEE International*, 2014, pp. 2C.1.1–2C.1.6.